Static Compression of Iron-Silicon Alloys: Implications for Silicon in the Earth's Core

Jung-Fu Lin[1], Andrew J. Campbell[1], Dion L. Heinz[1,2], Guoyin Shen[3]

[1]Department of the Geophysical Sciences, The University of Chicago, Chicago, IL 60637

[2]Also at James Franck Institute, The University of Chicago, Chicago, IL 60637

[3]Consortium for Advanced Radiation Sources, The University of Chicago, Chicago, IL 60637

ABSTRACT

Three iron-silicon alloys ($Fe_{85}Si_{15}$, $Fe_{71}Si_{29}$, and ε-FeSi) have been studied in a diamond anvil cell at room temperature up to 55 GPa by *in-situ* energy-dispersive X-ray diffraction techniques. A bcc to hcp phase transformation in $Fe_{85}Si_{15}$ began at 16 GPa and was completed by 36 GPa. No phase transformations are observed in either $Fe_{71}Si_{29}$ or ε-FeSi at high pressures, even when laser-heated to about 2000 K. The isothermal bulk modulus (K_{0T}) of hcp-$Fe_{85}Si_{15}$ is 141 (±10) GPa with K_{0T}'=5.70 (±0.60) and V_{02}=6.882 (±0.031) (cm^3/mol; per molar atoms). The K_{0T} of $Fe_{71}Si_{29}$ is 199.0 (±5.3) GPa with K_{0T}'=5.66 (±0.61) and V_0=6.687 (±0.014) (cm^3/mol), and the K_{0T} of ε-FeSi is 184.7 (±3.9) GPa with K_{0T}' of 4.75 (±0.37) and V_0=6.790 (±0.007) (cm^3/mol). Our study indicates that the substitution of Si into iron would lower the density of iron but does not significantly change its compressibility in the bcc phase, nor at high pressures in the hcp phase. Upon comparison with the Preliminary Reference Earth Model (PREM), the calculated equations of state (EOS) of hcp-$Fe_{85}Si_{15}$, using the Mie-Grüneisen EOS, indicate that an outer core containing about 8-10 wt% Si and inner core containing about 4 wt% Si in iron would satisfy the seismological constraints. Addition of silicon into iron increases the bulk sound velocity of iron, consistent with silicon being a light element in the Earth's core.

Introduction

Geophysical and cosmochemical evidence indicates that iron is the most abundant component in the Earth's core. The simplest interpretation of the core is an inner core composed of a crystalline iron-nickel alloy and an outer core of liquid iron-nickel alloyed with a small fraction of lighter element(s) (Birch, 1952). The density of the outer core is about 10% lower than the density of iron at core pressures and temperatures, while the bulk sound velocity of the core is about 3% higher than that of liquid iron (Birch, 1952; Dziewonski and Anderson, 1981; Ahrens, 1982; Anderson and Ahrens, 1994). The difference in density between the core and the high-pressure phase of iron indicates the presence of a low-atomic-weight component in the outer core (Birch, 1952). There is also evidence that the inner core is less dense than pure iron, and the amount of light element in the inner core may be as much as several weight percent (Jephcoat and Olson, 1987; Anderson and Ahrens, 1994; Stixrude et al., 1997; Fiquet et al., 2001; Mao et al., 2001). A number of light elements (H, C, N, O, Mg, Si, S) have been considered by various workers (e.g. Poirier, 1994; Hillgren et al., 2000).

Silicon has been proposed to be an important alloying element in the Earth's core, based on its cosmochemical abundance (Ringwood, 1966) and the thermoelastic properties of iron-silicon alloys in shock wave experiments (Balchan and Cowan, 1966;

Matassov, 1977). Allègre et al. (1995) used the ratios of major and trace elements in the mantle and in meteorite groups to estimate the possible silicon content in the core, and concluded that the core may contain about 7.3 wt% Si in addition to other light elements. Silicon solubility in liquid iron-rich metal increases with decreasing oxygen fugacity, increasing pressure, and increasing temperature, and a few weight percent of silicon may dissolve into liquid iron at the base of a deep magma ocean (~700 km depth, ~25 GPa) (Gessmann et al., 2001). To generate a core containing ~7.3 wt % Si as estimated by Allégre et al. (1995), a low oxygen fugacity during accretion (Ringwood, 1966) or possibly a magma ocean extending to 850 km (~30 GPa) (Gessmann et al., 2001) would be required. Studies of chemical reactions between mantle silicates and molten iron have also indicated that Fe-Si alloys may form at the core-mantle boundary (D" zone) (Knittle and Jeanloz, 1989; Knittle and Jeanloz, 1991). Shock experiments on Fe-Si alloys suggested that an outer core containing 14 to 20 wt% silicon in iron is sufficient to satisfy the density deficit of the core (Balchan and Cowan, 1966; Matassov, 1977).

Nevertheless, silicon was excluded as the primary alloying element in the outer core based on the relatively high bulk modulus (K_0) and low-pressure derivative of the bulk modulus (K_0') of an intermediate compound, iron silicide (ε-FeSi) (Knittle and Williams, 1995). Since the sound velocity of liquid iron is essentially parallel to the Preliminary

Reference Earth Model (PREM) velocity profile (Anderson and Ahrens, 1994), a lower value of K_0' of iron-silicon alloy would not be able to compensate for the effect of significant Si within the outer core (Williams and Knittle, 1997). In contrast, a recent static study on the equation of state (EOS) of a bcc-$Fe_{84}Si_{16}$ (in atomic percent) alloy up to 9 GPa and 773 K concluded that substitution of silicon in iron would not significantly change the compressibility of the iron-rich Fe-Si alloy (Zhang and Guyot, 1999).

Therefore, we studied the EOS of three Fe-Si alloys ($Fe_{85}Si_{15}$, $Fe_{71}Si_{29}$, and ε-FeSi) in a diamond anvil cell (DAC) to understand the elastic properties of various Fe-Si alloys under high pressures and to resolve the discrepancy between previous studies. We especially focused on the thermal EOS of iron-rich Fe-Si alloys because silicon alloyed with iron has a large effect upon the phase diagram of iron, and the iron-rich portion of the Fe-Si system is more applicable than ε-FeSi to understanding the possible effect of Si on iron under core conditions (Lin et al., 2002). The thermal EOS and bulk sound velocity of hcp-$Fe_{85}Si_{15}$ are calculated under core conditions, using our experimental data and the shock wave data. The $Fe_{71}Si_{29}$ and ε-FeSi alloys were also laser heated in a DAC to understand the stability of the phases under high pressures and high temperatures.

Experiments

The starting materials, $Fe_{85}Si_{15}$ alloy (lot# FE166010/6) and $Fe_{71}Si_{29}$ alloy (lot# FE176010/5), were purchased from Goodfellow Corporation and ε-FeSi (iron silicide; lot# C18G21) was obtained from Johnson Matthey. Electron microprobe analyses showed that the starting materials contained 7.9 (±0.3) wt% Si, 17.0 (±0.2) wt% Si, and 33.5 (±0.3) wt% Si (each averaged from at least 5 analyses), respectively. Angle-dispersive X-ray diffraction at ambient conditions showed that the $Fe_{85}Si_{15}$ was in body-centered cubic (bcc) structure with a=2.8520 (±0.0015) Å, $Fe_{71}Si_{29}$ was in the ordered B2 structure (space group: Pm3m) with a=2.8108 (±0.0020) Å, and ε-FeSi was in the B20 structure (space group: $P2_13$) with a=4.4846 (±0.0015) Å (Pauling and Soldate, 1948; Khalaff and Schubert, 1974; Kubaschewski, 1982). The B20 structure can be viewed as a distortion of the NaCl structure along [111] directions (Pauling and Soldate, 1948).

Stainless steel gaskets were pre-indented to a thickness of 30 μm and then drilled with a 100 μm hole. The sample was ground into a fine powder with an average grain size of 2 μm with gold powder added as the pressure standard (Heinz and Jeanloz, 1984a), and loaded into a DAC with ethanol-methanol (1:4) as the pressure medium. The mixture of ethanol-methanol pressure medium remains hydrostatic to almost 10 GPa; at high pressures it becomes a quasi-hydrostatic solid (Piermarini et al., 1973). Energy-dispersive synchrotron X-ray diffraction in a DAC was performed at Beamlines 13IDD

and 13BMD, GSECARS sector of the Advanced Photon Source (APS), Argonne National Laboratory (ANL). The X-ray beam was focused to less than a 10 μm spot onto the sample to minimize peak broadening caused by pressure gradients in the samples. Two clean-up slits, 30 μm in width, were used to cut off the tails of the focused X-ray beam. The energy calibration of the detector was accomplished using known energies of X-ray emission lines of several elements (Ag, Cd, and Co). The diffracted X-rays were collected by a Ge solid state detector at a fixed 2θ angle of about 8˚ or 12˚. The exposure times ranged from 5 to 10 minutes. The d-spacings of the sample and the internal standard were determined by fitting a Gaussian curve to each diffraction peak. Pressures were calculated from three to five diffraction lines from the set of (111), (200), (220), (311), and (222) for the gold standard (Heinz and Jeanloz, 1984a). Three to five diffraction peaks from the set of (100), (101), (102), (110), and (103) were used to calculate the unit cell parameters of hcp-$Fe_{85}Si_{15}$. Three to four diffraction peaks from the set of (100), (110), (200), and (211) were used to calculate the unit cell volume of $Fe_{71}Si_{29}$. Three to six diffraction lines from the set of (110), (111), (210), (211), (221), and (321) were used to calculate the unit cell parameters of ε-FeSi. Since all Fe-Si samples were in simple structures, the cell parameters of the samples were calculated

from the d-spacings. Standard deviations of the cell parameters were calculated from the variation of the d-spacings.

Since some of the X-ray diffraction peaks of Au overlapped with those of bcc-$Fe_{85}Si_{15}$, NaCl was mixed with the sample for use as a pressure calibrant in an externally heated diamond anvil cell up to 14 GPa to better measure the EOS of the bcc-$Fe_{85}Si_{15}$ (Birch, 1978; Bassett et al., 1993). The diffracted X-rays were collected at 300 K after the sample was annealed at about 800 K at high pressures to reduce the effects of nonhydrostaticity. Three diffraction peaks, (110), (200), and (211), were used to calculate the unit cell parameters for bcc-$Fe_{85}Si_{15}$.

The $Fe_{71}Si_{29}$ alloy (in ordered B2 structure) and the ε-FeSi alloy (in B20 structure) were laser heated in a DAC using the methods of Lin et al. (2002) to investigate the stability of these phases under high pressures and high temperatures. A sandwiched sample configuration, using NaCl as both the thermal insulator and pressure calibrant, was used in this study (Birch, 1978; Heinz and Jeanloz, 1984b).

Results

$Fe_{85}Si_{15}$, $Fe_{71}Si_{29}$, and ε-FeSi were compressed up to 54.3 GPa, 54.5 GPa, and 50.7 GPa, respectively (Figures 1,2,3,4). A phase transformation in the $Fe_{85}Si_{15}$ alloy from bcc

to hcp was observed to begin near 16 GPa and was completed by 36 GPa (Figures 1 and 2). The first appearance of the bcc phase during quench occurred at about 8 GPa, and the hcp phase can still be seen above 2 GPa (Figure 2). The two-phase (bcc+hcp) zone in $Fe_{85}Si_{15}$ extends over a wide pressure range of 20 GPa at 300 K, compared to 11 GPa for the same structural transition in iron (Huang et al., 1987). The volume change ($\Delta V/V_{01}$) across the bcc-hcp phase transition is about -1.9% or -0.13 cm^3/mol.

The pressure and volume data were analyzed with the Birch-Murnaghan equation of state (BM EOS) using a weighted least-squares linear fit of the strain (f) and the normalized stress (F) to obtain values for K_{0T} and K_{0T}' (Birch, 1978; Jeanloz, 1981) (Figure 5; Table 1-4). The isothermal EOS parameters are given in Table 5.

The $Fe_{71}Si_{29}$ and ε-FeSi alloys were laser heated up to ~1907 K at ~49 GPa and to ~2219 K at ~54 GPa, respectively. No phase transformation was observed in either sample, indicating that these silicon-rich Fe-Si alloys are relatively stable under high pressures and high temperatures.

Discussion

Isothermal compression at 300 K

Different results were reported in recent studies on the compressibility of ε-FeSi (Ross, 1994; Knittle and Williams, 1995; Sarrao et al., 1995; Wood et al., 1995; Guyot et al., 1997; Vocadlo et al., 1999) (Table 6). Most of the studies show that ε-FeSi has a bulk modulus between 160 GPa and 180 GPa. Our experimental technique and pressure range are similar to that used by Knittle and Williams (1995), but a significantly higher bulk modulus and lower pressure derivative of the bulk modulus is observed in their study. As shown in Figure 5d, their compression data are systematically higher than that of this study, indicating that the lower, incorrect lattice parameter (see Table 6) of V_0=6.701 ($\pm$0.032) (cm^3/mol) for ε-FeSi under ambient conditions used by Knittle and Williams (1995) significantly affects their results. Analyzing the static compression data of Knittle and Williams (1995) using V_0=6.790 ($\pm$0.007) (cm^3/mol) from this study, K_{0T} is found to be 155.6 (±4.6) GPa with K_{0T}'=6.31 (±0.78).

A plot of the molar volume of the Fe-Si alloys versus pressure (Figure 6) reveals that the compression curves of hcp-Fe, hcp-$Fe_{85}Si_{15}$, and ε-FeSi are almost identical to each other when extrapolated over 100 GPa, indicating that substitution of silicon into iron would lower the density of iron but has little effect on the volume and compressibility of iron alloys at high pressures. This result is consistent with conclusion of Zhang and

Guyot (1999) that substitution of Si in iron would not significantly change the compressibility of the iron-rich Fe-Si alloy.

Thermal EOS calculation

To estimate the simultaneous effects of pressure and temperature on the EOS of iron-rich Fe-Si alloys, we have calculated the thermal EOS of hcp-Fe and the hcp-$Fe_{85}Si_{15}$ alloy using the Mie-Grüneisen equation of state. Since bcc Fe-Si alloys have thermodynamic properties similar to those of iron under high pressures and high temperatures (Zhang and Guyot, 1999), it is reasonable to assume that hcp-$Fe_{85}Si_{15}$ also has thermodynamic parameters similar to those of hcp-Fe. The parameters used in calculating the EOS of hcp-Fe and hcp-$Fe_{85}Si_{15}$ in this study are listed in Table 7 (Matassov, 1977; Jeanloz, 1979; Jephcoat et al., 1986; Mao et al., 1990; Uchida et al., 2001). The Grüneisen parameter (γ_o) and $\partial \ln\gamma/\partial \ln V$ (q) of hcp-Fe measured by shock-wave experiments are used in this study (Jeanloz, 1979). The reference isotherm of hcp-Fe (Jephcoat et al., 1986; Mao et al., 1990; Uchida et al., 2001) and hcp-$Fe_{85}Si_{15}$ at 300 K is calculated using the BM EOS (Birch, 1978). The thermal EOS of Fe and $Fe_{85}Si_{15}$ is then calculated from the reference isotherm by use of the Mie-Grüneisen equation (McQueen et al., 1970):

$$P_i(V) = P_{300}(V) + \frac{\gamma}{V}[E_i(T_i,\Theta) - E_{300}(300,\Theta)] \quad (1)$$

where $P_{300}(V)$ is the pressure at the reference isotherm (300 K), γ is the Grüneisen parameter, V is the volume, Θ is the Debye temperature, and $E_i(T_i,\Theta)$ and $E_{300}(300, \Theta)$ are the thermal energies at temperatures T_i and 300 K, respectively. The thermal energies are calculated using:

$$E(T,\Theta) = (\frac{9nRT}{x^3}\int_0^x \frac{x^3}{e^x - 1}dx) + E_e \quad (2)$$

with

$$x = \frac{\Theta(V)}{T} \quad (3)$$

$$\gamma = \gamma_0(\frac{V}{V_0})^q = -\frac{d\ln\Theta}{d\ln V} \quad (4)$$

$$\Theta = \Theta_0 \exp^{\frac{\gamma_0}{q}[1-(\frac{V}{V_q})^q]} \quad (5)$$

Here E_e is the electronic contribution of the energy (Boness and Brown, 1986; Anderson and Ahrens, 1994), and the Grüneisen parameter and the Debye temperature are considered to be only functions of volume (Matassov, 1977), i.e. the quasi-harmonic approximation was used.

The electronic energy is:

$$E_e = \int_0^T C_e dT \quad (6)$$

where C_e is the electronic contribution to the heat capacity and T is the temperature. C_e data calculated by Boness and Brown (1986) are used both for Fe and $Fe_{85}Si_{15}$.

The reference adiabatic EOS is generated by using the BM EOS with $K_{0S} = K_{0T}(1+\alpha\gamma T)$ and K_{0S}'~K_{0T}' (Table 7). High-temperature adiabats are then calculated from the reference adiabat by use of the Mie-Grüneisen equation, and the temperature along each adiabat is:

$$T = T_0 \exp^{\frac{\gamma_0}{q}[1-(\frac{V}{V_0})^q]} \quad (7)$$

The Hugoniot curve is also calculated by use of the Mie-Grüneisen equation as follows (McQueen et al., 1970):

$$P_H = P_S + \frac{\gamma}{V}(E_H - E_S) \quad (8)$$

with

$$E_H = E_0 + \frac{(P_H + P_0)(V_0 - V)}{2} \quad (9)$$

$$E_S = E_0 - \int_{V_0}^{V} P_S dV \quad (10)$$

where P_H is the Hugoniot pressure, P_S is the pressure along the adiabat passing through P=0 GPa and T=300 K, E_H is the energy along the Hugoniot, E_S is the energy along the adiabat passing through P=0 GPa and T=300 K, and E_0, P_0, and V_0 are energy, pressure, and volume at the initial state, respectively. Thus, the Hugoniot pressure is:

$$P_H = \frac{P_S + \frac{\gamma}{V}\int_{V_0}^{V} P_S dV}{1 - \frac{\gamma}{2}(\frac{V_0}{V} - 1)} \quad (11)$$

The calculated Hugoniot curve from our data is consistent with shock wave experiments on $Fe_{87}Si_{13}$ (6.9 wt% Si) (Marsh, 1980) (Figure 7). The calculated adiabat passing through P=0 GPa and T=3000 K for hcp-$Fe_{85}Si_{15}$ shows that Fe-rich Fe-Si alloys have a lower density than pure iron under core conditions (Figure 8). Since melting has unobservable effect on the density of the solid and the liquid at a given pressure, the effect of melting on the density change should be less than a few percent (within the experimental error) at pressures relevant to the core (Jeanloz, 1979). Therefore, our calculated EOS of solid hcp-Fe and hcp-$Fe_{85}Si_{15}$ can be applied to discuss the density deficit of the liquid outer core.

Upon comparison with the PREM density profile (Figure 8), the calculated EOS of $Fe_{85}Si_{15}$ are consistent with an outer core containing Si as the light alloying element. An outer core containing about 8-10 wt% Si and an inner core containing about 4 wt% Si in iron can satisfy the density deficits in the core (Figure 8). Assuming a maximum silicon content in the core of 7.3 wt% (Allègre et al.,1995), a small amount of other light element(s) in addition to silicon may be needed to satisfy the density deficit of the outer core. However, the exact amount of the light element in the core depends on the

temperature profile of the core and the thermoelastic properties of the alloyed iron (Poirier, 1994; Hillgren et al., 2000).

Bulk sound velocity calculation

The bulk sound velocity of the core appears to be 3% higher than that of pure liquid iron (Ahrens, 1982; Anderson and Ahrens, 1994). The change of the bulk sound velocity across the liquid outer core to the solid inner core is small (Dziewonski and Anderson, 1981), suggesting that melting probably has small effect on the bulk sound velocity of iron under core conditions. High-pressure X-ray diffraction experiments on liquid Fe-Si alloy show that, in contrast to liquid Fe-S alloy (Sanloup et al., 2000), the presence of silicon in iron has negligible effect on the compressibility of iron (Sanloup et al., 2001). Therefore, if silicon is the dominant light element in the core, Fe-Si alloys must have higher bulk sound velocity than that of iron under core conditions. The bulk sound velocity is defined as:

$$V_\phi = \sqrt{\frac{K_S}{\rho}} \qquad (12)$$

where ρ is the density and K_S is the adiabatic bulk modulus. The adiabatic bulk modulus of iron-rich Fe-Si alloys at ambient conditions can be calculated from ultrasonic measurements of the elasticity of these alloys (Guinan and Beshers, 1968; Alberts and

Wedepohl, 1971; Routbort et al., 1971; Machova and Kadeckova, 1977). As shown in Figure 9, the adiabatic bulk modulus of the Fe-Si alloys in the bcc structure is independent of the silicon content and the shear modulus increases slightly with increasing the silicon concentration in the iron-rich Fe-Si alloys. As expected from the decrease in density of Fe-Si alloys, the bulk sound velocity, compressional wave velocity, and shear wave velocity of the iron-rich bcc Fe-Si alloys increase with increasing Si content (Figure 10). Addition of 8 wt% silicon increases the bulk sound velocity of bcc-Fe by approximately 3% (Figure 10). It was shown above that substitution of silicon in hcp-Fe would lower the density but would not significantly change the compressibility at high pressures; therefore addition of silicon into hcp-Fe would also increase the bulk sound velocity, consistent with silicon being a candidate light element in the core (Anderson and Ahrens, 1994).

The calculated bulk sound velocity of hcp-$Fe_{85}Si_{15}$ is higher than that of hcp-Fe under core conditions. However, the extrapolation of the bulk modulus to core conditions is compromised by the error on K_0' as well as the neglect of higher order coefficients (terms beyond 4^{th} order in strain) in the BM EOS. Precise experimental measurements on the elasticity and thermodynamic properties of Fe-Si alloys at higher pressure are needed in order to better constrain the bulk sound velocity of Fe-Si alloys under core conditions.

Conclusions

Candidate light elements in the core are restricted by the following three constraints: lower density than pure iron, higher bulk sound velocity than iron, and freezing point depression of iron under core conditions (Poirier, 1994; Yang and Secco, 1999; Hillgren et al., 2000). It has been demonstrated in this study that substitution of silicon in iron would lower the density but would not significantly change the compressibility of iron at high pressures. Silicon as the sole light alloying component in the core can produce a sufficiently large reduction in the density. Addition of silicon into iron increases the bulk sound velocity of iron, consistent with silicon being a candidate light element in the core. Finally, it is expected from the phase diagram of Fe-Si system at ambient pressure (Kusbaschewski, 1982) that addition of silicon into iron lowers the melting point of iron under these conditions. The melting temperatures observed for Fe17wt%Si up to 5.5 GPa are lower than those of pure iron (Yang and Secco, 1999).

Despite the previous exclusion of Si as the primary alloying element in the outer core based on the relatively high K_0 and low K_0' of ε-FeSi (Knittle and Williams, 1995; Williams and Knittle, 1997), our results based on the elasticity of three Fe-Si alloys ($Fe_{85}Si_{15}$, $Fe_{71}Si_{29}$, and ε-FeSi) indicate that silicon could be a significant light element in

the core. However, the possible presence of other light elements can not be excluded on the basis of these results.

Acknowledgments

We thank GSECARS at APS, ANL for providing the synchrotron beam and the William M. Keck Foundation for funding the facility. We also thank Dr. William Bassett, Dr. Eugene Huang, Mr. James Devine, and Ms. Wendy Mao for their assistance with the experiments and the manuscript and Dr. Ian Steele for his help with the electron microprobe analyses. This research is supported by NSF grant EAR-9974373 to D.L.H.

References

Ahrens, T. J., Constraints on core composition from shock-wave data, Phil. Trans. R. Soc. Lond. A, 306, 37-47, 1982.

Alberts, H. L., and P. T. Wedepohl, Elastic constants of dilute iron-silicon alloy single crystals below room temperature, Physica (Utrecht), 53, 571-580, 1971.

Allègre, C. J., J. P. Poirier, E. Humbler, and A. W. Hofmann, The chemical composition of the Earth, Earth Planet. Sci. Lett., 134, 515-526, 1995.

Anderson, W. W., and T. J. Ahrens, An equation of state for liquid iron and implications for the Earth's core, J. Geophys. Res., 99, 4273-4284, 1994.

Balchan, A. S., and G. R. Cowan, Shock compression of two iron-silicon alloys to 2.7 megabars, J. Geophys. Res., 71, 3577-3588, 1966.

Bassett, W. A., A. H. Shen, M. Bucknum, and I. M. Chou, Hydrothermal studies in a new diamond anvil cell up to 10 GPa and from –190 C to 1200 C, PAGEOPH, 141, 487-495, 1993.

Birch, F., Elasticity and constitution of the Earth's interior, J. Geophys. Res., 57, 227-286, 1952.

Birch, F., Finite strain isotherm and velocities for single-crystal and polycrystalline NaCl at high pressures and 300 K, J. Geophys. Res, 83, 1257-1268, 1978.

Boness, D. A. and J. M. Brown, The electronic thermodynamics of iron under Earth core conditions, Phys. Earth Planet. Inter., 42, 227-240, 1986.

Dziewonski, A. M., and D. L. Anderson, Preliminary reference Earth model, Phys. Earth Planet. Inter., 25, 297-356, 1981.

Fiquet G., J. Badro, F. Guyot, H. Requardt, and M. Krisch, Sound velocities in iron to 110 gigapascals, Science, 291, 468-471, 2001.

Gessmann, C. K., B. J. Wood, D. C. Rubie, and M. R. Kilburn, Solubility of silicon in liquid metal at high pressure: implications for the composition of the Earth's core, Earth Planet. Sci. Lett., 184, 367-376, 2001.

Guinan, M. W., and D. N. Beshers, Pressure derivatives of the elastic constants of α-iron to 10 kbs, J. Phys. Chem. Solids, 29, 541-549, 1968.

Guyot, F., J. Zhang, I. Martinez, J. Matas, Y. Ricard, and M. Javoy, P-V-T measurements of iron silicide (ε-FeSi): implications for silicate-metal interactions in the early Earth, Eur. J. Mineral., 9, 277-285, 1997.

Heinz, D.L., and R. Jeanloz, The equation of state of the gold calibration standard, J. Appl. Phys., 55, 885-893, 1984a.

Heinz, D.L., and R. Jeanloz, Compression of the B2 high-pressure phase of NaCl, Phys. Rev. B, 30, 6045-6050, 1984b.

Hillgren, V. J., C. K. Gessmann, and J. Li, An experimental perspective on the light element in Earth's core, in Origin of the Earth and the Moon, edited by R. M. Canup, K. Righter, pp. 245-263, The University of Arizona Press, Arizona, 2000.

Huang, E., W. A. Bassett, and P. Tao, Study of bcc-hcp iron phase transition by synchrotron radiation, in High-Pressure Research in Mineral Physics, edited by M. H. Manghnani and Y. Syono, pp. 165-172, TERRAPUB, Tokyo, 1987.

Jeanloz, R., Properties of iron at high pressures and the state of the core, J. Geophys. Res., 84, 6059-6069, 1979.

Jeanloz, R., Finite-strain equation of state for high-pressure phases, Geophys. Res. Lett., 8, 1219-1222, 1981.

Jephcoat, A., H. K. Mao, and P. M. Bell, Static compression of iron to 78 GPa with rare gas solids as pressure-transmitting media, J. Geophys. Res., 91, 4677-4684, 1986.

Jephcoat, A., and P. Olson, In the inner core of the Earth pure iron?, Nature, 325, 332-335, 1987.

Khalaff, K., and K. Schubert, Kristallstruktur von $Fe_2Si(h)$, J. Less-Common Met., 35, 341-345, 1974.

Knittle, E., and R. Jeanloz, Simulating the core-mantle boundary: an experimental study of high-pressure reactions between silicates and liquid iron, Geophys. Res. Lett., 16, 609-612, 1989.

Knittle, E., and R. Jeanloz, Earth's core-mantle boundary: results of experiments at high pressures and temperatures, Science, 251, 1438-1443, 1991.

Knittle, E., and Q. Williams, Static compression of ε-FeSi and evaluation of reduced silicon as a deep Earth constituent, Geophys. Res. Lett., 22, 445-448, 1995.

Kusbaschewski, O., Iron-binary phase diagram, Springer-Verlag, New York, 1982.

Lin, J. F., D. L. Heinz, A. J. Campbell, J. M. Devine, and G. Shen, Iron-silicon alloy in the Earth's core?, Science, 295, 313-315, 2002.

Machova, A., and S. Kadeckova, Elastic constants of iron-silicon alloy single crystals, Czech. J. Phys. B 27, 555-563, 1977.

Mao, H. K., Y. Wu, L. C. Chen, and J. F. Shu, Static compression of iron to 300 GPa and $Fe_{0.8}Ni_{0.2}$ alloy to 260 GPa: implications for composition of the core, J. Geophys. Res., 95, 21737-21742, 1990.

Mao, H. K. et al., Phonon density of states of iron up to 153 GPa, Science, 292, 914-916, 2001.

Marsh, S. P., LASL Shock Hugoniot Data, University of California Press, Berkeley, 1980.

Matassov, G., The electrical conductivity of iron-silicon alloys at high pressures and the Earth's core, Ph. D. thesis, Lawrence Livermore Laboratory Report #UCRL-52322, 1977.

McQueen, R. G., S. P. Marsh, J. P. Taylor, J. N. Fritz, and W. J. Carter, in High-Velocity Impact Phenomena, edited by R. Kinslow, Academic Press, New York and London, pp. 293-417, 1970.

Pauling, L., and A. M. Soldate, The nature of the bonds in the iron silicide FeSi and related crystals, Acta Cryst., 1, 212-216, 1948.

Piermarini, G. J., S. Block, and J. D. Barnett, Hydrostatic limits in liquids and solids to 100 kbar, J. Appl. Phys., 44, 5377-5382, 1973.

Poirier, J. P., Light elements in the Earth's core: a critical review, Phys. Earth Planet. Inter., 85, 319-337, 1994.

Ringwood, A. E., Chemical evolution of the terrestrial planets, Geochim. Cosmochim. Acta, 30, 41-104, 1966.

Ross, N. L., High-pressure single-crystal X-ray diffraction study of ε-FeSi, Acta Cryst. A52, C-530, 1994.

Routbort, J. L., C. N. Reid, E. S. Fisher, and D. J. Dever, High-temperature elastic constants and the phase stability of silicon-iron, Acta Met., 19, 1307-1316, 1971.

Sanloup, C. et al., Density measurements of liquid Fe-S alloys at high-pressure, Geophys. Res. Lett., 27, 811-814, 2000.

Sanloup, C. et al., Physical properties of liquid Fe alloys at high pressure and their bearings on the nature of metallic planetary cores: implications for the Earth, Mars and the Gailean satellites, Lunar Planet. Sci. XXXII, abstract 1877, 2001.

Sarrao, J. L., D. Mandrus, A. Migliori, Z. Fisk, and E. Bucher, Elastic properties of FeSi, Physica B, 199&200, 478-479, 1994.

Stixrude, L., E. Wasserman, and R. E. Cohen, Composition and temperature of Earth's inner core, J. Geophys. Res., 102, 24729-24739, 1997.

Uchida, T., Y. Wang, M. L. Rivers, and S. R. Sutton, Stability field and thermal equation of state of ε-iron determined by synchrotron X-ray diffraction in a multianvil apparatus, J. Geophys. Res., 106, 21799-21810, 2001.

Vocadlo, L., G. D. Price and I. G Wood, Crystal structure, compressibility and possible phase transitions in ε-FeSi studied by first-principles pseudopotential calculations, Acta Cryst., B55, 484-493, 1999.

Williams, Q., and E. Knittle, Constraints on core chemistry from the pressure dependence of the bulk modulus, Phys. Earth Planet. Inter., 100, 49-59, 1997.

Wood, I. G., T. D. Chaplin, W. I. F. David, S. Hull, G. D. Price, and J. N. Street, Compressibility of FeSi between 0 and 9 GPa, determined by high-pressure time-of-flight neutron powder diffraction, J. Phys. Condens. Matter, 7, L475-L479, 1995.

Yang, H., and R.A. Secco, Melting boundary of Fe-17%Si up to 5.5 GPa and the timing of core formation, Geophys. Res. Lett., 26, 263-266, 1999.

Zhang J. and F. Guyot, Thermal equation of state of iron and $Fe_{0.91}Si_{0.09}$, Phys. Chem. Minerals, 26, 206-211, 1999.

Table 1. Static compression data for bcc-$Fe_{85}Si_{15}$. a_o=2.8520 ($\pm$0.0015) Å and V_{01}=6.985 ($\pm$0.011) cm^3/mol at ambient conditions. The EOS of NaCl in B1 structure was used to determine the pressure (Birch, 1978).

Run#	P, GPa	std (P), GPa	a, Å	std (a), Å	V/V_{01}	std(V/V_{01})
Fe8Sieh445	4.00	0.06	2.8288	0.0020	0.9758	0.0021
Fe8Sieh437	6.30	0.09	2.8188	0.0022	0.9655	0.0023
Fe8Sieh310	7.20	0.11	2.8131	0.0012	0.9596	0.0012
Fe8Sieh311	8.20	0.12	2.8087	0.0002	0.9551	0.0002
Fe8Sieh303	8.50	0.13	2.8077	0.0012	0.9541	0.0012
Fe8Sieh429	8.64	0.13	2.8056	0.0012	0.9520	0.0012
Fe8Sieh428	10.62	0.16	2.7976	0.0004	0.9439	0.0004
Fe8Sieh420	11.02	0.17	2.7966	0.0016	0.9428	0.0016
Fe8Sieh401	11.12	0.17	2.7953	0.0010	0.9415	0.0010
Fe8Sieh412	11.55	0.17	2.7940	0.0009	0.9402	0.0009
Fe8Sieh301	11.91	0.18	2.7917	0.0005	0.9379	0.0005
Fe8Sieh406	13.50	0.20	2.7842	0.0010	0.9304	0.0010
Fe8Sieh407	13.60	0.20	2.7854	0.0001	0.9316	0.0001

Table 2. Static compression data for hcp-$Fe_{85}Si_{15}$. Data with asterisks were collected during the process of decreasing pressure. V_{02}/V_{01}=0.9851 ($\pm$0.0032). Au was used as the pressure calibrant (Heinz and Jeanloz, 1984a). File Fe79Si608 at 15.9 GPa was not included in the BM EOS fit because the X-ray peaks of hcp-$Fe_{85}Si_{15}$ were very weak.

Run#	P, GPa	std (P), GPa	a, Å	std (a), Å	c, Å	std (c), Å	V/V_{01}	std (V/V_{01})	c/a
Fe79Si636*	4.5	0.2	2.5040	0.0060	4.0890	0.0110	0.9571	0.0053	1.6330
Fe79Si635*	6.7	0.5	2.4980	0.0050	4.0540	0.0070	0.9444	0.0041	1.6229
Fe79Si547*	6.7	1.3	2.4923	0.0050	4.0502	0.0050	0.9392	0.0039	1.6251
Fe79Si634*	9.6	1.1	2.4890	0.0060	4.0080	0.0080	0.9269	0.0048	1.6103
Fe79Si608	15.9	0.8	2.4475	0.0050	3.9600	0.0050	0.8855	0.0038	1.6180
Fe79Si609	17.2	0.9	2.4535	0.0050	3.9691	0.0050	0.8918	0.0038	1.6177
Fe79Si633*	17.4	1.9	2.4570	0.0050	3.9720	0.0060	0.8951	0.0039	1.6166
Fe79Si545*	21.0	1.1	2.4406	0.0057	3.9947	0.0088	0.8883	0.0046	1.6368
Fe79Si610	21.0	1.2	2.4410	0.0060	3.9710	0.0060	0.8833	0.0045	1.6268
Fe79Si611	22.8	1.0	2.4380	0.0050	3.9450	0.0070	0.8754	0.0039	1.6181
Fe79Si612	24.0	1.2	2.4320	0.0100	3.9690	0.0160	0.8763	0.0080	1.6320
Fe79Si518	24.3	1.1	2.4345	0.0072	3.9612	0.0100	0.8764	0.0056	1.6271
Fe79Si519	24.5	1.3	2.4316	0.0063	3.9599	0.0080	0.8741	0.0049	1.6285
Fe79Si544*	24.7	1.2	2.4350	0.0059	3.9250	0.0068	0.8688	0.0045	1.6119
Fe79Si520	26.1	1.5	2.4262	0.0067	3.9447	0.0088	0.8668	0.0052	1.6259
Fe79Si613	26.5	1.2	2.4280	0.0060	3.9160	0.0070	0.8618	0.0045	1.6129
Fe79Si522	26.9	1.6	2.4260	0.0077	3.9292	0.0106	0.8633	0.0060	1.6196
Fe79Si521	27.0	1.5	2.4290	0.0078	3.9247	0.0108	0.8644	0.0060	1.6158
Fe79Si523	28.6	1.9	2.4208	0.0065	3.9236	0.0081	0.8584	0.0049	1.6208
Fe79Si614	29.1	1.4	2.4220	0.0060	3.9070	0.0070	0.8556	0.0045	1.6131
Fe79Si524	30.0	1.4	2.4201	0.0065	3.9182	0.0082	0.8567	0.0049	1.6190
Fe79Si632*	30.0	1.4	2.4270	0.0060	3.9030	0.0070	0.8582	0.0045	1.6082
Fe79Si615	31.5	1.6	2.4150	0.0060	3.8970	0.0070	0.8485	0.0045	1.6137
Fe79Si525	31.7	1.8	2.4135	0.0065	3.9076	0.0082	0.8497	0.0049	1.6191
Fe79Si543*	33.4	1.7	2.4197	0.0069	3.8899	0.0088	0.8502	0.0052	1.6076
Fe79Si526	33.8	1.9	2.4147	0.0069	3.9006	0.0089	0.8490	0.0052	1.6154
Fe79Si616	34.6	1.7	2.4090	0.0060	3.8890	0.0080	0.8425	0.0045	1.6144
Fe79Si527	34.8	1.7	2.4009	0.0080	3.9013	0.0085	0.8395	0.0059	1.6249
Fe79Si528	36.4	1.9	2.3989	0.0073	3.8965	0.0077	0.8371	0.0054	1.6243
Fe79Si617	37.0	1.8	2.4000	0.0060	3.8890	0.0070	0.8362	0.0044	1.6204
Fe79Si529	38.1	2.1	2.3952	0.0075	3.8898	0.0079	0.8331	0.0055	1.6240
Fe79Si618	39.1	2.0	2.3950	0.0060	3.8790	0.0070	0.8306	0.0044	1.6196
Fe79Si530	39.4	2.1	2.3891	0.0078	3.8893	0.0082	0.8287	0.0057	1.6279
Fe79Si542*	39.9	2.0	2.3912	0.0072	3.8825	0.0075	0.8287	0.0052	1.6237
Fe79Si619	40.8	2.1	2.3930	0.0060	3.8730	0.0070	0.8279	0.0044	1.6185
Fe79Si531	41.0	2.1	2.3850	0.0081	3.8792	0.0086	0.8237	0.0059	1.6265
Fe79Si620	42.2	2.3	2.3880	0.0060	3.8670	0.0070	0.8232	0.0044	1.6193
Fe79Si631*	44.4	2.5	2.3880	0.0060	3.8540	0.0070	0.8204	0.0044	1.6139
Fe79Si621	44.4	2.5	2.3840	0.0050	3.8440	0.0080	0.8156	0.0038	1.6124
Fe79Si622	45.9	2.6	2.3810	0.0060	3.8480	0.0070	0.8144	0.0044	1.6161
Fe79Si533	45.9	2.4	2.3733	0.0064	3.8745	0.0065	0.8147	0.0046	1.6325
Fe79Si534	46.3	2.5	2.3711	0.0052	3.8768	0.0052	0.8137	0.0037	1.6350
Fe79Si541*	46.6	2.5	2.3742	0.0061	3.8466	0.0102	0.8094	0.0047	1.6202
Fe79Si623	48.1	2.7	2.3790	0.0050	3.8400	0.0060	0.8113	0.0036	1.6141
Fe79Si624	48.6	2.7	2.3780	0.0050	3.8370	0.0060	0.8100	0.0036	1.6135
Fe79Si535	49.1	2.8	2.3715	0.0067	3.8486	0.0086	0.8080	0.0049	1.6229
Fe79Si625	50.3	2.8	2.3740	0.0050	3.8330	0.0060	0.8064	0.0036	1.6146

Fe79Si536	50.5	2.8	2.3705	0.0060	3.8596	0.0073	0.8096	0.0044	1.6282
Fe79Si630*	50.7	2.9	2.3740	0.0050	3.8330	0.0060	0.8064	0.0036	1.6146
Fe79Si626	51.4	2.9	2.3710	0.0050	3.8270	0.0060	0.8031	0.0036	1.6141
Fe79Si537	51.8	2.9	2.3701	0.0061	3.8268	0.0102	0.8025	0.0047	1.6146
Fe79Si539*	52.9	3.1	2.3683	0.0065	3.8145	0.0080	0.7987	0.0047	1.6106
Fe79Si627	52.9	3.0	2.3690	0.0050	3.8190	0.0050	0.8001	0.0035	1.6121
Fe79Si538	53.3	3.1	2.3674	0.0063	3.8132	0.0076	0.7978	0.0045	1.6107
Fe79Si628	54.1	3.1	2.3680	0.0050	3.8130	0.0060	0.7982	0.0036	1.6102
Fe79Si629	54.3	3.1	2.3680	0.0050	3.8190	0.0060	0.7994	0.0036	1.6128

Table 3. Static compression data for $Fe_{71}Si_{29}$. a_0=2.8108 (±0.0020) Å. Au was used as the pressure calibrant (Heinz and Jeanloz, 1984a).

Run#	P, GPa	std (P), GPa	a, Å	std(a), Å	V/V_0	std (V/V_0)
Fe17Si401	2.8	0.3	2.7994	0.0025	0.9879	0.0026
Fe17Si402	2.9	0.3	2.7992	0.0026	0.9877	0.0028
Fe17Si403	3.1	0.4	2.7979	0.0028	0.9863	0.0030
Fe17Si502	3.6	0.7	2.7916	0.0055	0.9796	0.0058
Fe17Si404	4.2	0.3	2.7934	0.0014	0.9815	0.0015
Fe17Si405	5.4	0.3	2.7876	0.0022	0.9754	0.0023
Fe17Si406	7.0	0.4	2.7819	0.0017	0.9695	0.0018
Fe17Si407	8.1	0.3	2.7771	0.0020	0.9645	0.0021
Fe17Si408	10.5	0.4	2.7691	0.0025	0.9562	0.0026
Fe17Si409	11.8	0.6	2.7602	0.0020	0.9470	0.0021
Fe17Si410	14.0	0.6	2.7508	0.0019	0.9373	0.0019
Fe17Si412	17.0	1.1	2.7408	0.0020	0.9271	0.0020
Fe17Si413	18.9	1.3	2.7387	0.0030	0.9250	0.0030
Fe17Si414	21.5	1.1	2.7330	0.0014	0.9192	0.0014
Fe17Si415	22.7	0.9	2.7270	0.0036	0.9132	0.0036
Fe17Si507	24.6	1.0	2.7306	0.0055	0.9168	0.0055
Fe17Si416	24.9	1.2	2.7214	0.0018	0.9076	0.0018
Fe17Si423*	26.3	1.2	2.7233	0.0062	0.9095	0.0062
Fe17Si417	26.5	1.3	2.7176	0.0051	0.9038	0.0051
Fe17Si418	27.5	1.5	2.7140	0.0049	0.9002	0.0049
Fe17Si419	30.1	1.9	2.7058	0.0048	0.8921	0.0047
Fe17Si420	31.5	2.1	2.7023	0.0047	0.8886	0.0046
Fe17Si422*	32.6	1.9	2.7035	0.0041	0.8898	0.0040
Fe17Si421	33.8	1.8	2.6966	0.0048	0.8830	0.0047
Fe17Si510	40.0	2.0	2.6884	0.0049	0.8750	0.0048
Fe17Si511	47.4	2.4	2.6739	0.0039	0.8609	0.0038
Fe17Si512	54.5	2.7	2.6613	0.0025	0.8488	0.0024

Table 4. Static compression data for ε-FeSi. a_o=4.4846 (±0.0015) Å. Au was used as the pressure calibrant (Heinz and Jeanloz, 1984a).

Run#	P, GPa	std (P), GPa	a, Å	std(a), Å	V/V_0	std (V/V_0)
FeSi201	0.6	0.1	4.4840	0.0018	0.9996	0.0012
FeSi101	1.2	0.3	4.4768	0.0038	0.9948	0.0025
FeSi134*	1.5	0.7	4.4834	0.0046	0.9992	0.0031
FeSi102	1.5	0.3	4.4743	0.0042	0.9931	0.0028
FeSi219*	1.6	0.3	4.4781	0.0024	0.9957	0.0016
FeSi202	1.9	0.4	4.4695	0.0071	0.9899	0.0047
FeSi103	4.1	0.2	4.4524	0.0025	0.9786	0.0016
FeSi203	4.2	0.5	4.4464	0.0064	0.9747	0.0042
FeSi204	6.9	0.2	4.4267	0.0049	0.9618	0.0032
FeSi104	7.5	0.7	4.4312	0.0035	0.9647	0.0023
FeSi218*	8.1	0.4	4.4387	0.0042	0.9696	0.0028
FeSi205	9.5	0.4	4.4077	0.0046	0.9494	0.0030
FeSi105	10.0	0.9	4.4168	0.0038	0.9553	0.0025
FeSi133*	10.1	0.5	4.4243	0.0048	0.9602	0.0031
FeSi132*	10.3	0.5	4.4232	0.0049	0.9595	0.0032
FeSi206	12.5	0.5	4.3881	0.0040	0.9368	0.0026
FeSi106	13.5	0.6	4.3971	0.0044	0.9426	0.0028
FeSi207	17.5	1.0	4.3678	0.0043	0.9239	0.0027
FeSi108	18.3	1.2	4.3690	0.0021	0.9246	0.0013
FeSi107	18.7	1.0	4.3694	0.0026	0.9249	0.0017
FeSi208	22.4	0.9	4.3472	0.0048	0.9109	0.0030
FeSi109	23.6	1.0	4.3400	0.0043	0.9064	0.0027
FeSi209	23.7	1.0	4.3368	0.0049	0.9044	0.0031
FeSi110	23.9	1.0	4.3316	0.0046	0.9011	0.0029
FeSi215*	24.0	1.1	4.3465	0.0049	0.9104	0.0031
FeSi111	25.9	1.3	4.3175	0.0073	0.8923	0.0045
FeSi210	27.1	1.2	4.3238	0.0048	0.8962	0.0030
FeSi113	29.1	1.8	4.3105	0.0040	0.8880	0.0025
FeSi130*	29.3	1.7	4.2948	0.0019	0.8783	0.0012
FeSi214*	29.6	1.7	4.3108	0.0054	0.8882	0.0033
FeSi112	32.6	1.7	4.2889	0.0049	0.8747	0.0030
FeSi211	32.7	1.8	4.2917	0.0070	0.8764	0.0043
FeSi114	32.9	1.7	4.2890	0.0040	0.8748	0.0024
FeSi213*	33.1	1.6	4.2927	0.0083	0.8770	0.0051
FeSi115	33.3	1.8	4.2932	0.0024	0.8773	0.0015
FeSi212	34.3	1.8	4.2894	0.0077	0.8750	0.0047
FeSi116	36.4	2.2	4.2698	0.0104	0.8631	0.0063
FeSi118	37.0	1.9	4.2859	0.0102	0.8729	0.0062
FeSi129*	38.8	2.3	4.2608	0.0092	0.8576	0.0056
FeSi117	40.2	2.3	4.2586	0.0102	0.8563	0.0062
FeSi119	43.4	3.5	4.2559	0.0090	0.8547	0.0054
FeSi122	44.2	2.2	4.2525	0.0072	0.8526	0.0043
FeSi121	44.9	2.3	4.2492	0.0045	0.8506	0.0027
FeSi124	45.7	2.5	4.2410	0.0076	0.8457	0.0045
FeSi127*	45.8	2.3	4.2454	0.0032	0.8484	0.0019
FeSi128*	45.9	2.4	4.2472	0.0096	0.8494	0.0058
FeSi123	46.2	2.8	4.2420	0.0049	0.8463	0.0029
FeSi120	46.8	3.8	4.2517	0.0051	0.8522	0.0031
FeSi126*	48.3	2.4	4.2387	0.0084	0.8444	0.0050
FeSi125	50.7	2.5	4.2279	0.0040	0.8379	0.0024

Table 5. EOS parameters of bcc-$Fe_{85}Si_{15}$, hcp-$Fe_{85}Si_{15}$, $Fe_{71}Si_{29}$, and ε-FeSi.

Composition	V_0 (cm^3/mol)	Structure	K_{0T}	K_{0T}'	Highest pressure, GPa
$Fe_{85}Si_{15}$	6.986 (±0.007)	bcc	157.8 (±4.0)	5.26 (±0.88)	13.6
$Fe_{85}Si_{15}$	6.882 (±0.031)	hcp	141 (±10)	5.70 (±0.60)	54.3
$Fe_{71}Si_{29}$	6.687 (±0.014)	B2	199.0 (±5.3)	5.66 (±0.61)	54.5
ε-FeSi	6.790 (±0.007)	B20	184.7 (±3.9)	4.75 (±0.37)	50.7

Table 6. Comparison of the elastic parameters of ε-FeSi.

Reference	Pressure range	K_0 (GPa)	K_0'	V_0 (cm^3/mol)	Technique
This study	51 GPa	185 (±4)	4.8 (±0.4)	6.790 (±0.007)	X-ray diffraction in DAC
Ross (1994)	7 GPa	176 (±3)	4 (fixed)	n.a.	Single-crystal X-ray diffraction
Knittle & Williams (1995)	50 GPa	209 (±6)	3.5 (±0.4)	6.701 (±0.032)	X-ray diffraction in DAC
Sarrao et al. (1994)	room pressure	173*	n.a.	n.a.	Ultrasonic spectroscopy
Wood et al. (1995)	9 GPa	160 (±1)	4 (fixed)	6.794 (±0.01)	Neutron diffraction
Guyot et al. (1997)	8 GPa	172 (±3)	4 (fixed)	6.805 (±0.005)	X-ray diffraction in multi-anvil apparatus
Vocadlo et al. (1999)	calculation	227	3.9	6.692	First-principle calculations

* indicates the adiabatic bulk modulus

Table 7. Thermodynamic properties of hcp-Fe and hcp-$Fe_{85}Si_{15}$ at ambient conditions.

Variable		hcp-Fe	Remark	hcp-Fe8wt%Si	Remark
Molar volume	V_0	6.84 ($\pm$0.01) cm^3	Uchida et al, 1990	6.88($\pm$0.03) cm^3	This study
Isothermal bulk modulus	K_{0T}	135 ($\pm$19) GPa	"	141($\pm$10) GPa	"
Pressure derivative of K_{OT}	K_{0T}'	6.0 ($\pm$0.4)	"	5.70($\pm$0.6)	"
*Adiabatic bulk modulus	K_{0S}	140 ($\pm$20) GPa	Calculated	146 ($\pm$10) GPa	Calculated
†Heat capacity	C_v	23.1 ($\pm$6.2) $Jmol^{-1}K^{-1}$	Calculated	24.3 ($\pm$5.8) $Jmol^{-1}K^{-1}$	Calculated
‡Thermal expansion	α	5.5 ($\pm$0.4) $x10^{-5}$ K^{-1}	Uchida et al., 2001	5.5 ($\pm$0.4) $x10^{-5}$ K^{-1}	Asssumed
Debye temperature	Θ	464 K	Matassov, 1977	421 K	Matassov, 1977
‡Gruneisen parameter	γ_o	2.2 ($\pm$0.5)	Jeanloz, 1979	2.2 ($\pm$0.5)	Assumed
‡($\partial\ln\gamma/\partial\ln V$)	q	1.62 ($\pm$0.37)	Jeanloz, 1979	1.62 ($\pm$0.37)	"

* K_{0S} is calculated from $K_{0S}=K_{0T}(1+\alpha\gamma T)$

† C_v is calculated from $C_v=\alpha K_{0T}V/\gamma$

‡ Thermal expansion coefficient, Grüneisen parameter and $\partial\ln\gamma/\partial\ln V$ of hcp-$Fe_{85}Si_{15}$ are assumed to be the same as that of hcp-Fe

FIGURE CAPTIONS:

Figure 1. A series of X-ray diffraction patterns of $Fe_{85}Si_{15}$ at increasing pressures to 54.3 GPa and then at decreasing pressures at 300 K. Diffraction peaks from the bcc and hcp phases of the alloy are indicated. F, the fluorescence peaks of gold; Au, the internal pressure calibrant.

Figure 2. A plot of d-spacing versus pressure for $Fe_{85}Si_{15}$ alloy under high pressures at 300 K. When the pressure was elevated above 16 GPa, a transformation to a hcp phase was clearly observed (indicated as hcp in). This phase transition was completed by 36 GPa (indicated as bcc out). The first appearance of the bcc phase during the quench process occurred at about 8 GPa (bcc in), and the hcp phase can still be seen above 2 GPa (hcp out). Open circles, bcc phase in increasing pressure; solid circles, bcc phase in decreasing pressure; open triangles, hcp phase in increasing pressure; solid triangles, hcp phase in decreasing pressure.

Figure 3. A series of X-ray diffraction patterns of $Fe_{71}Si_{29}$ at increasing pressures to 47.4 GPa at 300 K. Diffraction peaks from the $Fe_{71}Si_{29}$ phase are shown as bold. F, the fluorescence peaks of gold; Au, the internal pressure calibrant.

Figure 4. A series of X-ray diffraction patterns of ε-FeSi at increasing pressures to 34.3 GPa at 300 K. F, the fluorescence peaks of gold; Au, the internal pressure calibrant.

Figure 5. (a) Relative volume of bcc-$Fe_{85}Si_{15}$ as a function of pressure at 300 K. Dashed line represents a weighted least-squares fit. **(b)** Relative volume of the hcp-$Fe_{85}Si_{15}$ as a function of pressure at 300 K. **(c)** Relative volume of the $Fe_{71}Si_{29}$ as a function of pressure at 300 K. **(d)** Relative volume of the ε-FeSi as a function of pressure at 300 K (solid circles). Compression data for ε-FeSi collected by Knittle and Williams (1995) are also plotted for comparison (open circles). A lower V_0 used by Knittle and Williams (1995) may cause the systematic discrepancy between the compression data.

Figure 6. Comparison of molar volume (per unit molar atoms) versus pressure at 300 K for hcp-Fe, hcp-$Fe_{85}Si_{15}$, and ε-FeSi. Crosses: hcp-Fe (Jephcoat et al., 1986; Mao et al., 1990; Uchida et al., 2001); open circles: hcp-$Fe_{85}Si_{15}$; open squares: ε-FeSi in B20 structure (extrapolated from this study); dashed line: ε-FeSi extrapolated from Knittle and Williams (1995).

Figure 7. Hugoniot for hcp-$Fe_{85}Si_{15}$ alloy. Solid line: 300K BM EOS of the hcp-$Fe_{85}Si_{15}$; dashed line: calculated Hugoniot; open circles: shock wave data for $Fe_{87}Si_{13}$ (Marsh, 1980); crosses: static compression data for hcp-$Fe_{85}Si_{15}$ (this study).

Figure 8. Calculated adiabats of hcp-Fe and hcp-$Fe_{85}Si_{15}$ compared to the PREM model. The temperature for the adiabat of the hcp-$Fe_{85}Si_{15}$ passing through P=0 GPa and T=3000 K at the core-mantle boundary is about 4948 K and is about 6300 K at inner core-outer core boundary. Thick black line: PREM; thin black line: an adiabat passing through P=0

GPa and T=300 K for hcp-Fe; dashed black line: an adiabat passing through P=0 GPa and T=3000 K for hcp-Fe; thin gray line: an adiabat passing through P=0 GPa and T=300 K for hcp-$Fe_{85}Si_{15}$; dashed gray line: an adiabat passing through P=0 GPa and T=3000 K for hcp-$Fe_{85}Si_{15}$.

Figure 9. Adiabatic bulk moduli (open circles) and shear moduli (open squares) calculated from ultrasonic measurements of the elasticity of the iron-rich Fe-Si alloys at ambient conditions (Guinan and Beshers, 1968; Alberts and Wedepohl, 1971; Routbort et al., 1971; Machova and Kadeckova, 1977). All alloys were in bcc structure.

Figure 10. Bulk sound velocities (open circles), compressional wave velocities (open diamonds), and shear wave velocities (open triangles) of iron-rich Fe-Si alloys calculated from ultrasonic measurements at ambient conditions (Guinan and Beshers, 1968; Alberts and Wedepohl, 1971; Routbort et al., 1971; Machova and Kadeckova, 1977).

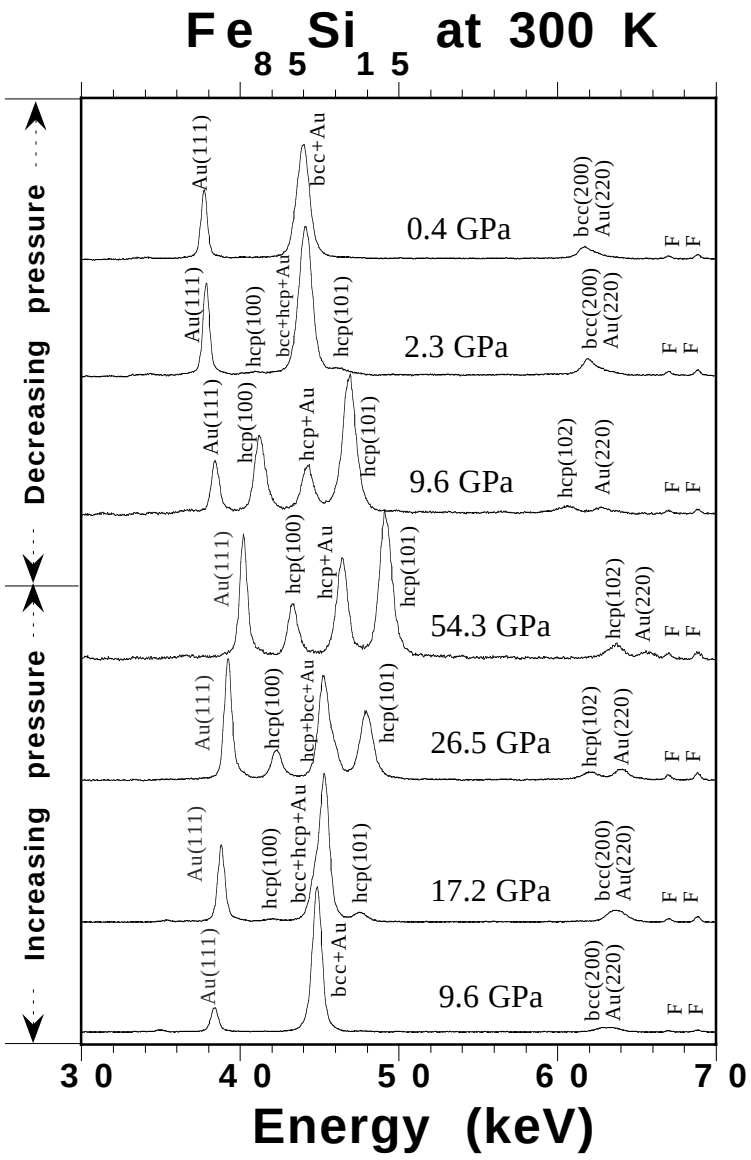
Fe85Si15 at 300 K
Decreasing pressure
Increasing pressure
0.4 GPa
2.3 GPa
9.6 GPa
54.3 GPa
26.5 GPa
17.2 GPa
9.6 GPa
Au(111)
bcc+Au
bcc(200)
Au(220)
F
hcp(100)
bcc+hcp+Au
hcp(101)
hcp+Au
hcp(102)
hcp+bcc+Au
bcc+hcp+Au
30
40
50
60
70
Energy (keV)

Figure 1

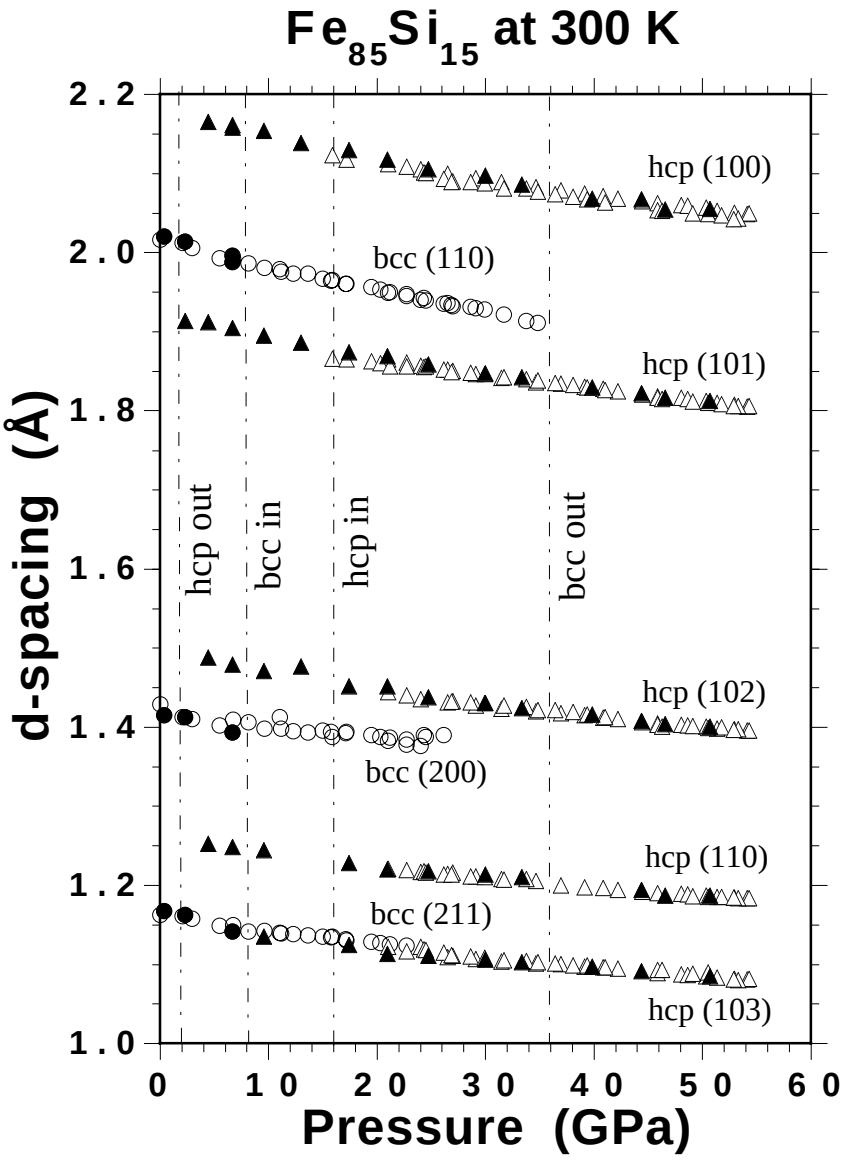
Fe85Si15 at 300 K
d-spacing (Å)
Pressure (GPa)
2.2
2.0
1.8
1.6
1.4
1.2
1.0
0
10
20
30
40
50
60
hcp out
bcc in
hcp in
bcc out
hcp (100)
bcc (110)
hcp (101)
hcp (102)
bcc (200)
hcp (110)
bcc (211)
hcp (103)

Figure 2

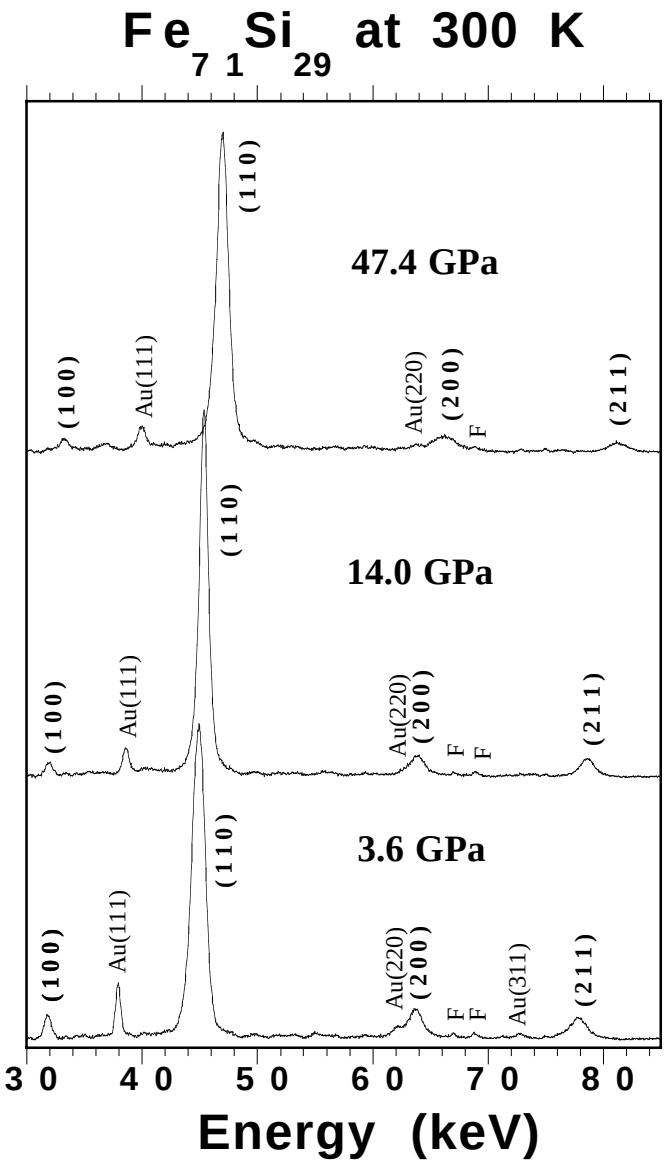
Fe71Si29 at 300 K
47.4 GPa
14.0 GPa
3.6 GPa
(100)
Au(111)
(110)
Au(220)
(200)
F
F
(211)
Au(311)
30
40
50
60
70
80
Energy (keV)

Figure 3

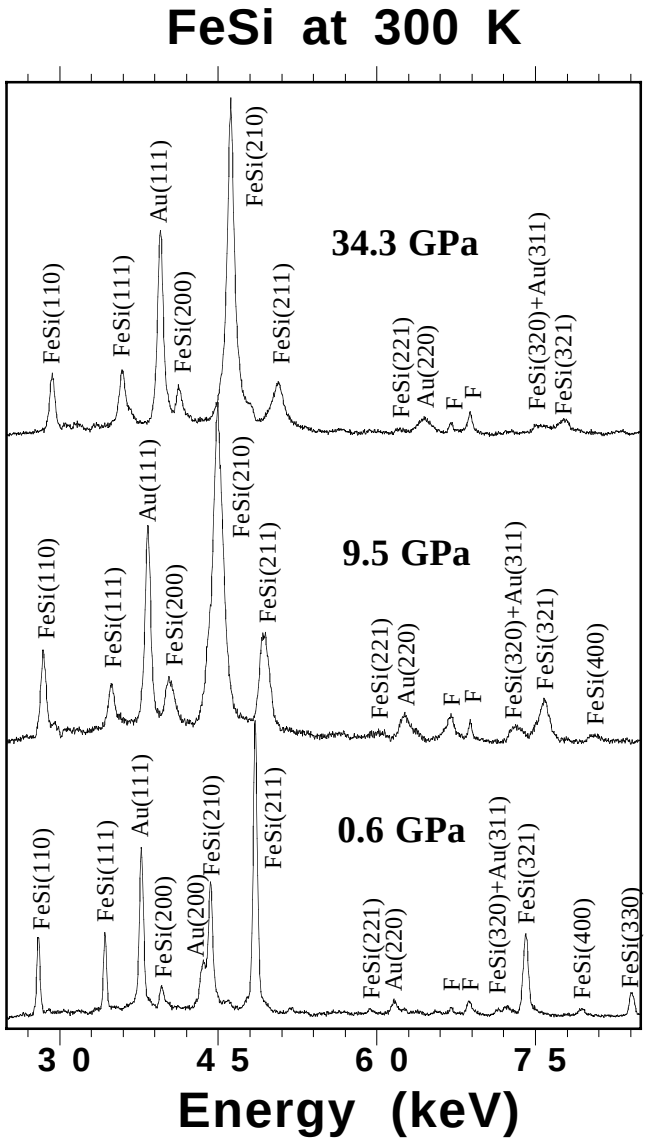
FeSi at 300 K
34.3 GPa
FeSi(110)
FeSi(111)
Au(111)
FeSi(200)
FeSi(210)
FeSi(211)
FeSi(221)
Au(220)
F
F
FeSi(320)+Au(311)
FeSi(321)
9.5 GPa
FeSi(110)
FeSi(111)
Au(111)
FeSi(200)
FeSi(210)
FeSi(211)
FeSi(221)
Au(220)
F
F
FeSi(320)+Au(311)
FeSi(321)
FeSi(400)
0.6 GPa
FeSi(110)
FeSi(111)
Au(111)
FeSi(200)
Au(200)
FeSi(210)
FeSi(211)
FeSi(221)
Au(220)
F
F
FeSi(320)+Au(311)
FeSi(321)
FeSi(400)
FeSi(330)
3 0
4 5
6 0
7 5
Energy (keV)

Figure 4

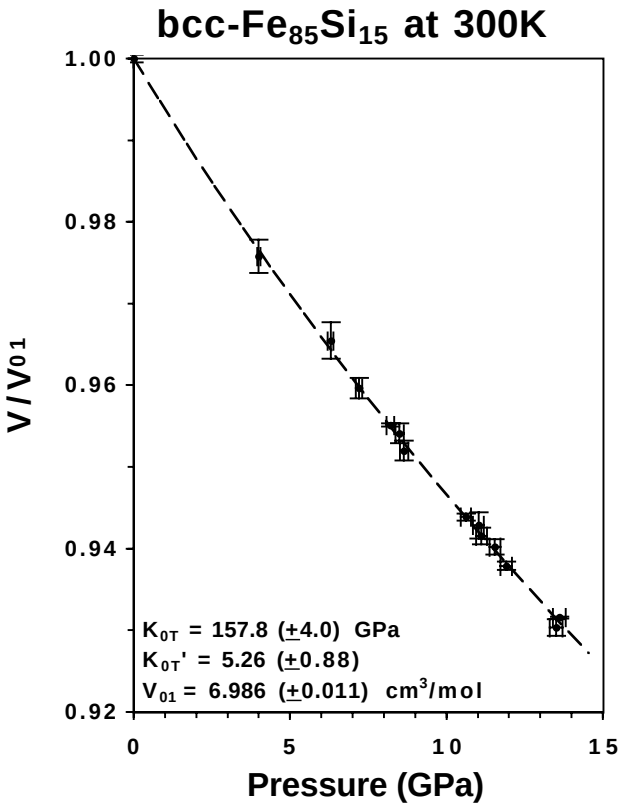
bcc-Fe85Si15 at 300K
1.00
0.98
0.96
0.94
0.92
V / V01
0
5
10
15
Pressure (GPa)
K0T = 157.8 (±4.0) GPa
K0T' = 5.26 (±0.88)
V01 = 6.986 (±0.011) cm3/mol

Figure 5a

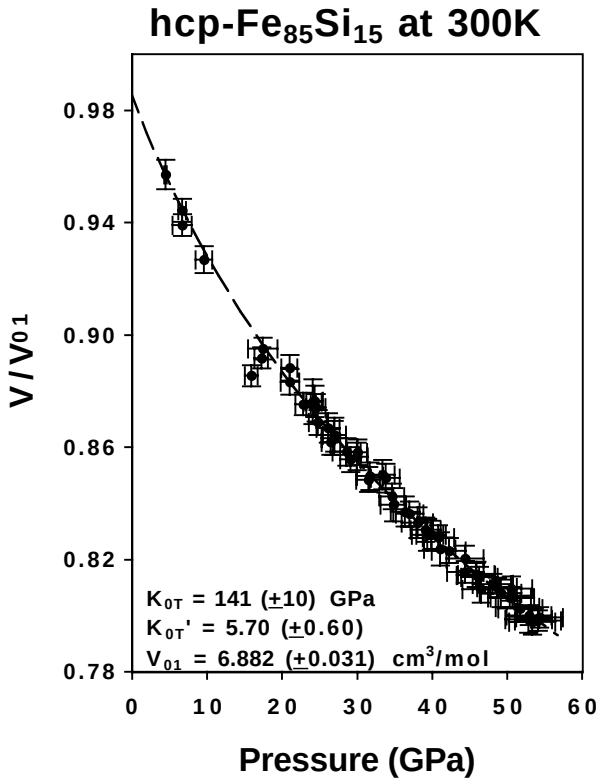
hcp-Fe85Si15 at 300K
V / V01
0.98
0.94
0.90
0.86
0.82
0.78
0
10
20
30
40
50
60
Pressure (GPa)
K0T = 141 (±10) GPa
K0T' = 5.70 (±0.60)
V01 = 6.882 (±0.031) cm3/mol

Figure 5b

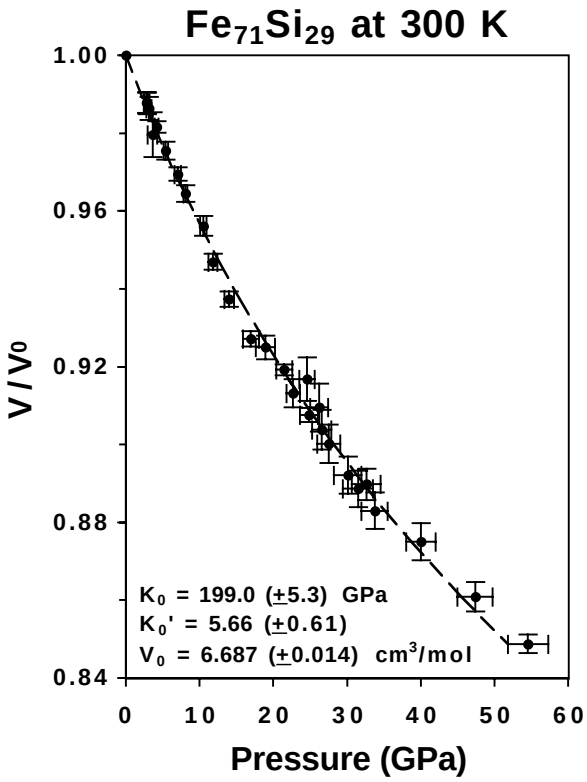
Fe71Si29 at 300 K
1.00
0.96
0.92
0.88
0.84
V / V0
K0 = 199.0 (±5.3) GPa
K0' = 5.66 (±0.61)
V0 = 6.687 (±0.014) cm3/mol
0
10
20
30
40
50
60
Pressure (GPa)

Figure 5c

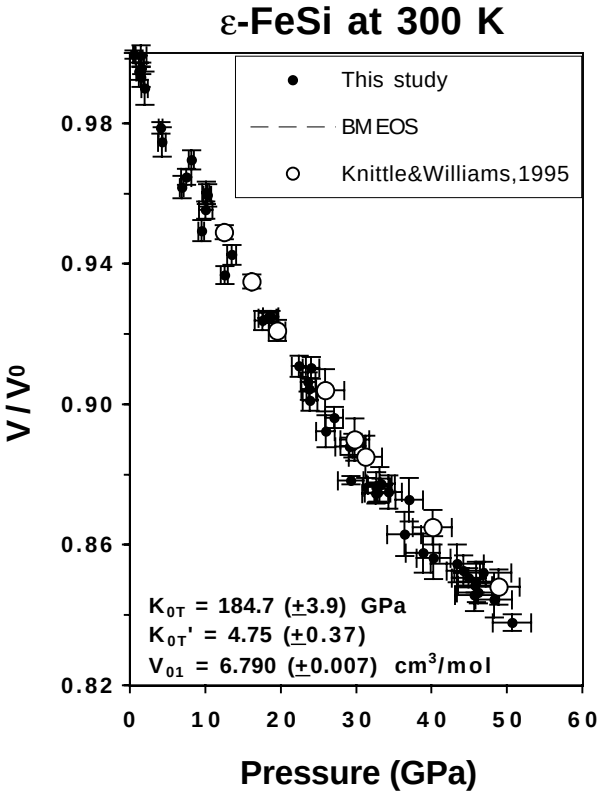
ε-FeSi at 300 K
This study
BM EOS
Knittle&Williams,1995
V / V0
0.98
0.94
0.90
0.86
0.82
0
10
20
30
40
50
60
Pressure (GPa)
K0T = 184.7 (±3.9) GPa
K0T' = 4.75 (±0.37)
V01 = 6.790 (±0.007) cm3/mol

Figure 5d

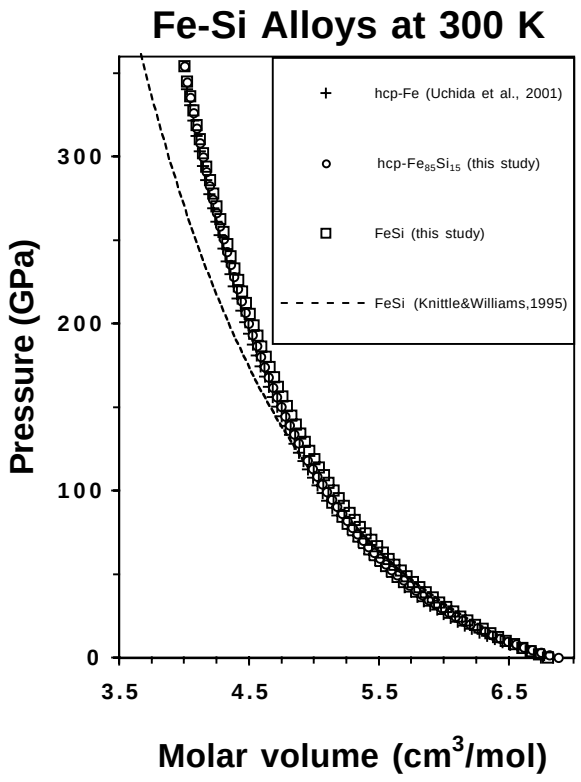
Fe-Si Alloys at 300 K
hcp-Fe (Uchida et al., 2001)
hcp-Fe85Si15 (this study)
FeSi (this study)
FeSi (Knittle&Williams,1995)
Pressure (GPa)
0
100
200
300
3.5
4.5
5.5
6.5
Molar volume (cm3/mol)

Figure 6

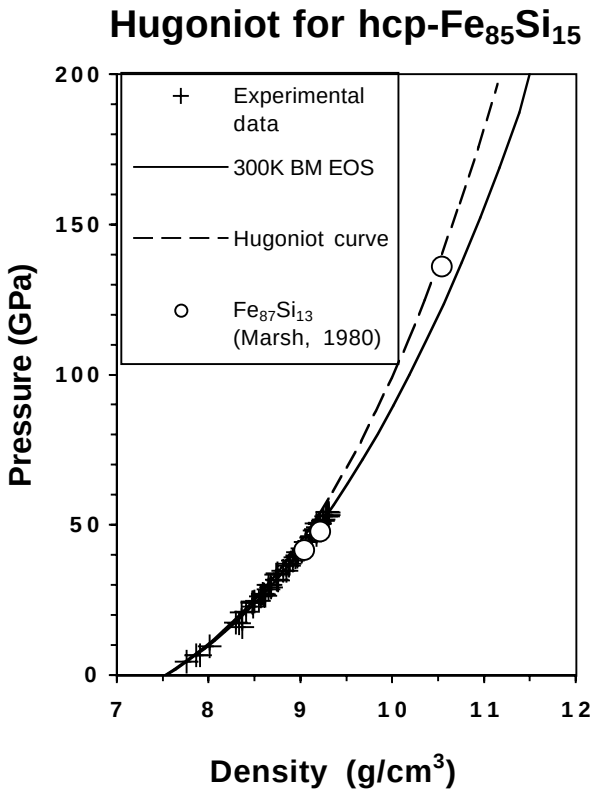
Hugoniot for hcp-Fe85Si15
Experimental data
300K BM EOS
Hugoniot curve
Fe87Si13 (Marsh, 1980)
Pressure (GPa)
Density (g/cm3)
0
50
100
150
200
7
8
9
10
11
12

Figure 7

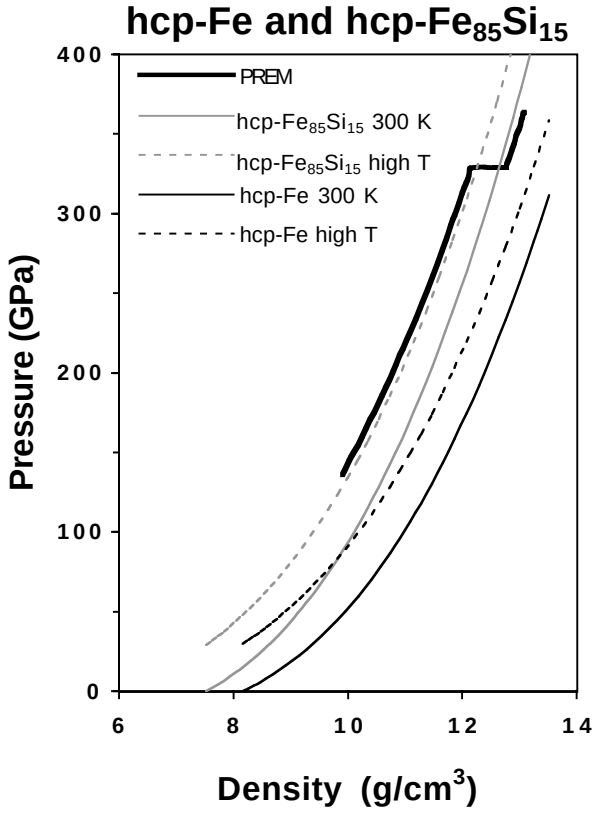
hcp-Fe and hcp-Fe85Si15
PREM
hcp-Fe85Si15 300 K
hcp-Fe85Si15 high T
hcp-Fe 300 K
hcp-Fe high T
Pressure (GPa)
400
300
200
100
0
6
8
10
12
14
Density (g/cm3)

Figure 8

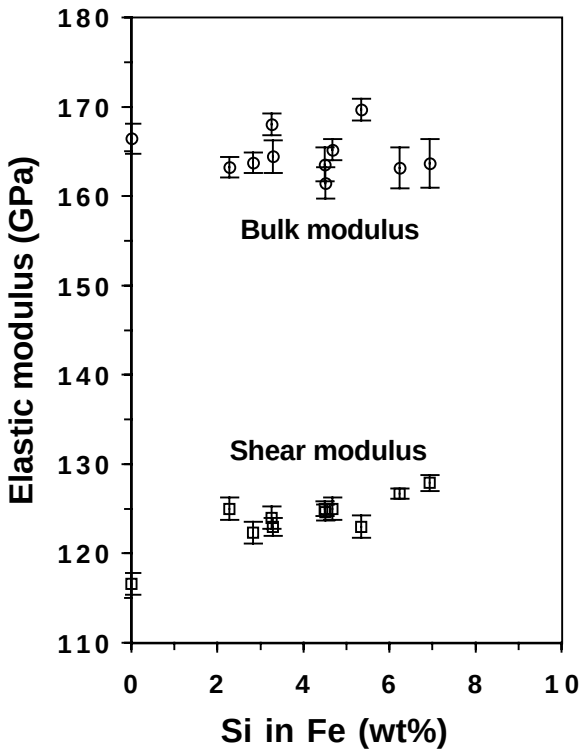
Elastic moduli of Fe-Si alloys at 300 K
Elastic modulus (GPa)
180
170
160
150
140
130
120
110
Bulk modulus
Shear modulus
0
2
4
6
8
10
Si in Fe (wt%)

Figure 9

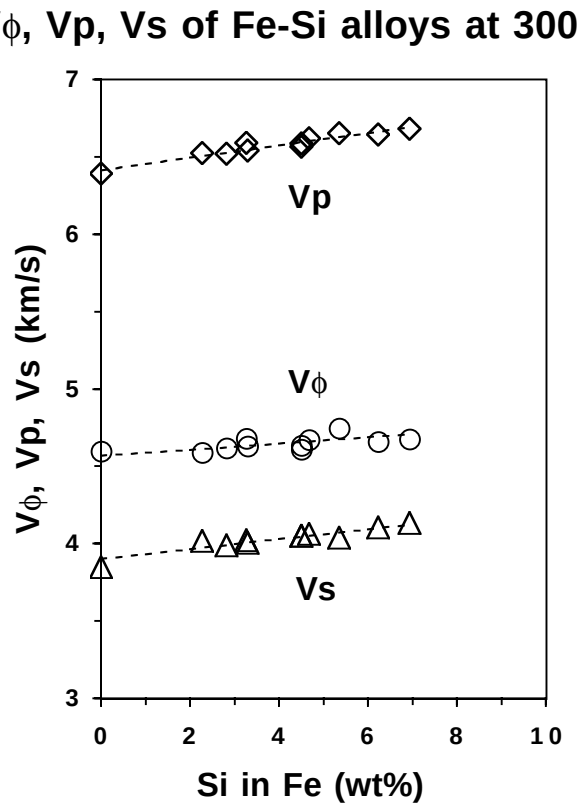
Vϕ, Vp, Vs of Fe-Si alloys at 300 K
Vp
Vϕ
Vs
Vϕ, Vp, Vs (km/s)
Si in Fe (wt%)
7
6
5
4
3
0
2
4
6
8
10

Figure 10

Supplementary Table 1 Observed energy-dispersive X-ray diffraction peaks of bcc-$Fe_{85}Si_{15}$ and NaCl (pressure calibrant) at 11.91 (±0.18) GPa and 300 K (Run number: Fe8Sieh301). The unit cell parameter of the bcc and NaCl are 2.7917 (±0.0005) Å and 5.1750 (±0.0006) Å, respectively.

h	k	l	d-spacing (Å)	d_{obs}-d_{cal} (Å)	FWHM (Å)	Phase
2	0	0	2.5872	-0.0003	0.0312	NaCl
1	1	0	1.9736	-0.0004	0.0344	bcc
2	2	0	1.8298	0.0002	0.0210	NaCl
2	0	0	1.3959	0.0001	0.0358	bcc
4	0	0	1.2938	0.0001	0.0111	NaCl
2	1	1	1.1399	0.0002	0.0194	bcc

Supplementary Table 2 Observed energy-dispersive X-ray diffraction peaks of hcp-$Fe_{85}Si_{15}$ and Au (pressure calibrant) at 53.3 (±3.1) GPa and 300 K (Run number: Fe79Si538). The unit cell parameters of the hcp-$Fe_{85}Si_{15}$ structure are: a= 2.3674 (±0.0063) Å, c= 3.8132 (±0.0076) Å, and c/a= 1.6107. The unit cell parameter of Au is 3.8283 (±0.0023) Å.

h	k	l	d_{obs} (Å)	d_{obs}-d_{cal} (Å)	FWHM (Å)	Phase
1	1	1	2.2122	0.0019	0.0347	Au
1	0	0	2.0435	-0.0068	0.0377	hcp
2	0	0	1.9137	-0.0004	0.0386	Au
1	0	1	1.8065	0.0007	0.0325	hcp
1	0	2	1.3971	0.0009	0.0337	hcp
2	2	0	1.3528	-0.0007	0.0200	Au
1	1	0	1.1840	0.0003	0.0167	hcp
2	2	2	1.1050	-0.0002	0.0139	Au
1	0	3	1.0801	-0.0002	0.0172	hcp

Supplementary Table 3 Observed energy-dispersive X-ray diffraction peaks of $Fe_{71}Si_{29}$ and Au (pressure calibrant) at 24.6 (±1.0) GPa and 300 K (Run number: Fe17Si507). The unit cell parameters of $Fe_{71}Si_{29}$ and Au are 2.7306 (±0.0055) Å and 3.9326 (±0.0012) Å, respectively.

h	k	l	d-spacing (Å)	FWHM (Å)	d_{obs}-d_{cal} (Å)	Phase
1	1	1	2.2710	0.0452	0.0005	Au
1	1	0	1.9352	0.0398	0.0044	$Fe_{71}Si_{29}$
2	0	0	1.3637	0.0355	-0.0016	$Fe_{71}Si_{29}$
2	1	0	1.2186	0.0131	-0.0026	$Fe_{71}Si_{29}$
3	1	1	1.1855	0.0125	-0.0003	Au
2	1	1	1.1159	0.0264	0.0012	$Fe_{71}Si_{29}$

Supplementary Table 4 Observed energy-dispersive X-ray diffraction peaks of ε-FeSi and Au (pressure calibrant) at 24.0 (±1.1) GPa and 300 K (Run number: FeSi215). The unit cell parameters of ε-FeSi and Au are 4.3465 (±0.0049) Å and 3.9354 (±0.0023) Å, respectively.

h	k	l	d-spacing (Å)	FWHM (Å)	d_{obs}-d_{cal} (Å)	Phase
1	1	0	3.0793	0.0675	0.0059	ε-FeSi
1	1	1	2.2730	0.0349	0.0009	Au
1	1	1	2.5064	0.1002	-0.0031	ε-FeSi
2	0	0	2.1748	0.0729	0.0015	ε-FeSi
2	1	0	1.9427	0.0379	-0.0011	ε-FeSi
2	1	1	1.7738	0.0519	-0.0007	ε-FeSi
2	2	0	1.3908	0.0217	-0.0006	Au
3	2	1	1.1612	0.0145	-0.0005	ε-FeSi